The Astrophysical Journal Supplement Series, 230:7 (18pp), 2017 May https://doi.org/10.3847/1538-4365/aa6df9

An Accurate Flux Density Scale from 50 MHz to 50 GHz

R. A. Perley and B. J. Butler
National Radio Astronomy Observatory, P.O. Box O, Socorro, NM 87801, USA; RPerley@nrao.edu, BButler@nrao.edu
Received 2016 September 19; revised 2017 April 11; accepted 2017 April 13; published 2017 May 19

Abstract

The flux-density scale of Perley & Butler is extended downward to ∼50 MHz by utilizing recent observations with the Karl G. Jansky Very Large Array (VLA)[1] of 20 sources between 220 MHz and 48.1 GHz, and legacy VLA observations at 73.8 MHz. The derived spectral flux densities are placed on an absolute scale by utilizing the Baars et al. values for Cygnus A (3C405) for frequencies below 2 GHz, and the Mars-based polynomials for 3C286, 3C295, and 3C196 from Perley & Butler above 2 GHz. Polynomial expressions are presented for all 20 sources, with accuracy limited by the primary standards to 3%–5% over the entire frequency range. Corrections to the scales proposed by Perley & Butler, and by Scaife & Heald are given.

Key words: instrumentation: interferometers – methods: data analysis – methods: observational – techniques: interferometric – telescopes

Supporting material: machine-readable table

1. Introduction

The radio astronomy flux-density scale has long been based on the polynomial expressions given in Baars et al. (1977) for four "absolute" and 13 "secondary" sources. The members of the first group—Cygnus A, Casseopeia A, Taurus A, and Virgo A—all have angular extents of arcminutes and high spectral flux densities, typically in excess of 1000 Jy at $\lambda = 1$ m. They are sufficiently strong for their flux densities to be accurately measured with low-resolution telescopes with known gains, but their large-scale structure makes them unsuitable for calibration by high-resolution interferometric arrays. The members of the second group are much smaller—typically 10 s of arcseconds or less, and weaker, with typical flux densities of less than 50 Jy at $\lambda = 1$ m. The flux densities at low frequencies of these weaker sources could not be accurately measured by single antennas of known gain, primarily because of background source confusion, and were determined by taking ratios against the members of the first group, using higher resolution arrays. A subset of these "secondary" sources, comprising the smallest among them, has been extensively utilized for flux-density calibration of interferometers in the meter–centimeter wavelength range.

The Baars et al. (1977; hereafter Baars77) scale for the compact ("secondary") sources is nominally valid between 0.4 and 15 GHz with an accuracy of ∼5%. Prior to ∼1990, the great majority of observing with the Very Large Array (VLA) was at its two lowest frequency bands—1.5 and 5 GHz, so there was little incentive to extend the Baars77 flux-density scale above 15 GHz. After that time, the VLA's 15 and 23 GHz receivers were replaced with much more sensitive ones, and a new band, centered at 45 GHz was added. These additions, and the subsequent holographic surface adjustments and improvements in observing methodologies needed to support high frequency VLA observing, resulted in a greatly increased use of high frequencies on the VLA, necessitating the extension of the Baars77 scale to higher frequencies. Accurate measurements of a set of small-diameter radio sources by the VLA resulted in the Perley & Butler (2014; herafter PB14) scale, which was placed on an absolute scale via VLA and *WMAP* observations of the planet Mars, utilizing a thermophysical model of that planet's emission. The PB14 scale is valid between 1 and 50 GHz, with a claimed accuracy of ∼1% over the central frequencies, rising to ∼3% at the highest and lowest frequencies.

Over the past decade, there has been an upsurge in interest in, and development of, low-frequency radio astronomy. However, the Baars77 scale for the compact objects useful for calibration purposes is not defined below 400 MHz. Indeed, the low-frequency flux-density scale has long been quite uncertain, as summarized in the Baars77 paper. Table 7 of that paper shows the ratio of their scale for the "absolute" sources to the scales of Conway et al. (1963), Kellermann (1964), Baars et al. (1965), Baars & Hartsuijker (1983), and Wills (1973). Variations at the ∼10% level are seen—most likely due to the effects of background source confusion to the low-resolution instruments utilized at the time. A useful low-frequency scale has been proposed by Scaife & Heald (2012; hereafter SH12), valid between 30 and 300 MHz. This work is a rationalization of 13 different, but interlinked, flux-density scales. The SH12 scale adopts the B77 scale above 325 MHz, and the Roger et al. (1973) scale below 325 MHz. The correction factors needed to adjust the 13 scales to those adopted for the SH12 scale are given in their Table 2—some are as large as 20%. Given the renewed interest in low-frequency astronomy, placing the low-frequency flux-density scale on a firm footing, using modern telescopes, is a worthy endeavor.

Accurately placing the low-frequency flux-density scale onto an absolute standard requires a highly linear, high-resolution array, preferably comprised of high-gain elements, capable of cleanly separating the proposed calibration targets from surrounding emission. As demonstrated by PB14, the VLA is easily capable of determining ratios between proposed calibration sources to ∼1% accuracy at its low-frequency bands. Placing the results on an absolute scale requires a highly linear correlator because the only suitable "absolute" reference source over the 0.02–2 GHz range is Cygnus A, whose flux density

[1] The National Radio Astronomy Observatory is a facility of the National Science Foundation operated under cooperative agreement by Associated Universities, Inc.

exceeds those of the proposed secondary calibrators by more than two orders of magnitude. The original VLA was ill-suited to this task becuase its digital correlator was not sufficiently linear over the large range of correlation coefficients to directly bootstrap the standard calibrators to Cygnus A.[2] This situation changed in 2012, with the commissioning of the Jansky VLA, and its new correlator, which uses a 4-bit (16 level) correlation. The result of this was that the response to the absolute standard source Cygnus A can now be safely linked to weaker—and smaller—radio sources suitable for the calibration for interferometers.

Most of the previous work on the flux density scales has been limited to northern sources, with few southern sources reliably linked to the absolute standards. In view of the development of numerous southern-hemisphere low-frequency arrays, it is important to rectify this situation by inclusion of southern sources.

In this paper, we propose a single flux-density scale, valid from 50 MHz through 50 GHz, based on new observations with the VLA of 19 proposed calibrator sources, over the frequency range of 230 MHz to 48 GHz, located in both hemispheres, along with "legacy" observations of 13 sources with the VLA at 73.8 MHz.

2. Observations

The results presented here are taken from a more general instrumental program whose primary goal is to determine and track the VLA's instrumental parameters over all nine frequency bands. The source lists were drawn from the Baars77, PB14, and SH12 papers, with six additional southern-hemisphere objects added to assist in extending the northern flux calibrator grid to the south. The six additional southern sources were selected primarily to assist calibration of the new low-frequency low-resolution southern-hemisphere arrays—MWA, PAPER, and HERA. Are all large-diameter sources that are primarily useful for flux-density bootstrapping at low frequencies. Not all sources were observed at all bands—the large angular extent of many of the selected sources makes observing them with the VLA impractical at high frequencies.

For notational brevity, we will utilize "band codes" to represent the various receiver systems employed on the VLA. These codes are defined in Table 1.

The source list, and the bands utilized for each source, are given in Table 2.

The observations were made in five observing sessions on the dates listed in Table 3, which also gives the time spent in each session, and the array configuration in which the observations were made.

The first two of these sessions were taken under Project ID AK461, whose goal was to survey the major 3C sources as part of the commissioning of the initial "4-band" (73 MHz) receiving system (Kassim et al. 2007). These data were taken with the original VLA correlator, with 1.6 MHz bandwidth.[3] All other data were taken with the new Jansky VLA system.

Table 1
Band Codes

Band Code	Representative Wavelength	Frequency Span (MHz)
4[a]	4 m	73.0–74.6
P[a]	90 cm	224–480
L	20 cm	1000–2000
S	10 cm	2000–4000
C	5 cm	4000–8000
X	3 cm	8000–12000
Ku	2 cm	12000–18000
K	13 mm	18000–26500
Ka	9 mm	26500–40000
Q	7 mm	40000–50000

Note.
[a] The VLA's low-frequency system now comprises a single receiver covering 50–480 MHz and two feeds, covering 50–80, and 224–480 MHz, respectively. The 90 cm observations described here are taken with this new system. The 4 m observations described here are from the narrowband "legacy" system (Kassim et al. 2007), which is now disabled.

The observations taken in 2016 January were to provide more short spacings for better determination of the flux densities of the highly extended sources in the target list. Frequency tuning details are given in Table 4.

Although the new data were taken with the wideband system, not all spectral windows were utilized, as the smoothness of the synchrotron emission process requires only a reasonable sampling of the spectrum to enable an accurate description. The center frequencies of the spectral windows utilized in the analysis are given in Table 4. Note that all but one of the SPWs in the P-band system were utilized,[4] primarily to assist in the verification of the new low-band system. The center frequencies listed at the P band are not uniformly separated by 16 MHz (the SPW spacing)—this reflects the flagging necessary to remove RFI-affected channels.

To provide an extra level of calibration, periodic observations of three far northern sources—J0217+7349, J1153+8058, and J1800+7828—were added at all frequency bands except "4" and "P." These were included since their near-constant elevation, and 24 hr availability, allow for easier separation of temporal from elevation gain dependencies, should the on-board gain calibration system not function as needed. As described below, this was indeed the case for some bands.

3. Observation and Calibration Methodology

The methodology employed is identical to that described in PB14, and will not be described in detail here. In summary, observations of the sources were taken in all nine VLA observing bands over the course of a day. Each observation was short—less than 30 s—so that typically 6–10 observations (roughly hourly) of each source, at each band, are available for analysis. The repetition permits the correction of various effects, such as the sensitivity and elevation gain dependency of each band, and provides statistically valid determinations of the source flux densities. Correlator dump times were kept short—1 s—to permit detailed editing. Editing and calibration methods were identical to those described in PB14.

[2] For Cygnus A, the correlation coefficient at 300 MHz through 1500 MHz is over 0.7—which is well beyond the linear range for the VLA's original three-level correlator.

[3] Note that, at 73.8 MHz, the extremely low efficiency of the VLA's antennas (∼0.15), combined with the extremely high sky temperature (∼8000 K) result in a correlation coefficient for Cygnus A of only 5%, well within the safe linear range of the old correlator. Hence, we are able to utilize "legacy" observations for this work.

[4] The only one not utilized, at 264 MHz, was lost to RFI.

Table 2
Source List

Name	Alternate Names	4	P	L	S	C	X	Ku	K	Ka	Q	LAS[a](arcsec)
J0133−3629			•	•								900
J0137+3309	3C48	•	•	•	•	•	•	•	•	•	•	1.2
J0322−3712	Fornax A		•	•								3000
J0437+2940	3C123	•	•	•	•	•	•	•	•	•	•	43
J0444−2809			•	•								120
J0519−4546	Pictor A		•	•	•							480
J0521+1638	3C138		•	•	•	•	•	•	•	•	•	0.65
J0534+2200	3C144, Taurus A, Crab	•	•	•	•	•						480
J0542+4951	3C147	•	•	•	•	•	•	•	•	•	•	0.70
J0813+4813	3C196	•	•	•	•	•	•	•	•	•	•	6.0
J0918−1205	3C218, Hydra A	•	•	•	•	•	•	•				420
J1230+1223	3C274, Virgo A, M87	•	•	•	•							840
J1331+3030	3C286	•	•	•	•	•	•	•	•	•	•	3.5
J1411+5212	3C295	•	•	•	•	•	•	•	•	•	•	6.5
J1651+0459	3C348, Hercules A		•	•	•	•	•					195
J1720−0058	3C353	•	•	•	•							320
J1829+4844	3C380	•	•	•	•	•	•	•	•	•	•	18
J1959+4044	3C405, Cygnus A	•	•	•	•	•	•					110
J2214−1701	3C444		•	•	•	•	•					120
J2323+5848	3C461, Cassiopeia A	•	•	•	•							480

Note.
[a] LAS = Largest Angular Size.

Table 3
Observing Log

Date	IAT Start hh:mm	LST Start hh:mm	Duration hr	Configuration	Comments
1998 Mar 07–08	17:45	21:30	24	A	4-band only
1998 Oct 04–05	12:15	06:00	24	B	4-band only
2014 Oct 11–12	01:00	19:10	30	C	
2016 Jan 25–26	05:00	06:10	27	DnC	D to C reconfig.
2016 Jan 27	01:00	02:10	5	DnC	D to C reconfig.

Table 4
Observing Frequencies

Band Code	Frequency Span MHz	SPW Width MHz	Frequencies Used MHz
4	73.0–74.6	1.625	73.8
P	224–480	16	232, 247, 275, 296, 312, 328, 344, 357, 382, 392, 403, 422, 437, 457, 471
L	1008–2032	64	1040, 1488, 1808
S	1988–3012, 2988–4012	128	2052, 2948
C	4188–5212, 5988–7012	128	4764, 6564
X	7888–8912, 10488–11512	128	8592, 11064
Ku	13488–14512, 15988–17012	128	14192, 16564
K	18488–19512, 24988–26012	128	19065, 25564
Ka	31488–32512, 36488–37512	128	32064, 37064
Q	41488–42512, 47488–48512	128	42064, 48064

Note. The Jansky VLA electronics provides two parallel independently tuned analog channels. At the "P" band, only one of these was utilized. At the "L" band the two channels, each 512 MHz wide, were arranged to be adjacent. At all other bands, the two channels were separated, with frequency ranges as given in the second column. The "SPW Width" column gives the effective bandwidth of the data used for the flux-density determinations.

Accurate flux-density measurements require accurate correction for instrumental gain variations. There are two principal sources of time-variable gains for VLA observations—temperature-induced receiver gain changes, and elevation-dependent gains changes caused by deformation of the primary reflector. The first affects all bands, the second is only appreciable at wavelengths shorter than 6 cm. At the VLA's higher frequencies, these effects are of approximately equal magnitude, so accurate calibration requires an electronics gain monitor, which is independent of the antenna elevation. For this purpose, the VLA's receivers include a switched power monitoring system whose output accurately tracks receiver gain

Table 5
Derived Spectral Flux Densities

Freq	J0133	%Err
.073	⋯	0.5
.232	25.2	1.6
.247	19.5	1.0
.275	24.2	0.3
.296	19.7	0.2
.312	22.5	0.7
.328	21.6	0.2
.344	19.6	0.3
.357	19.6	0.3
.382	18.1	0.4
.392	18.9	0.5
.403	19.6	0.5
.422	19.1	0.4
.437	17.7	0.7
.457	17.8	0.6
.471	17.9	0.6
1.040	10.3	0.5
1.488	8.18	0.5
1.808	7.15	0.5
2.052	6.58	0.4
2.948	4.93	0.5
3.670	⋯	0.5
4.764	⋯	0.5
6.564	⋯	0.6
8.592	⋯	0.4
11.064	⋯	0.5
14.192	⋯	0.5
16.564	⋯	0.5
19.064	⋯	0.6
25.564	⋯	0.7
32.064	⋯	0.8
37.064	⋯	0.7
42.064	⋯	0.8
48.064	⋯	4.7

(This table is available in its entirety in machine-readable form.)

changes. Application of these data removes the gain variations due to the electronics with an accuracy of ∼1%, and permits accurate measurement of the variation of antenna gain with elevation.

However, application of this gain monitioring data could not be done for those observations, which included the four strongest "absolute" sources—notably Cygnus A, the primary flux-density calibrator—as it has been found that for sources such as this, which typically multiply the total power in the system by a factor of ∼4, the switched power monitor system falsely reports a small, but significant, drop in gain. This effect is seen in all receivers except for the low-frequency system. Hence, in the calibration, the switched power system was utilized only for the four highest-frequency bands, for which no attempt to link the standard calibrators to Cygnus A was made, and at P-band, where the false compression is not detected.

This phenomenon was known to exist in advance of these observations, thus to allow an alternate route for removal of the amplifier gain variations, observations of three far northern sources, whose average elevation remains nearly constant, once every 4 hr was included. This is a sufficient cadence, since receiver gain changes (including the temperature-driven contribution) typically vary on timescales longer than this. The three sources were always observed sequentally.

Following correction for the temporal amplifier gain changes, the elevation gain dependency, and flux densities of the target sources was determined in the manner described in PB14.

3.1. Generation of Flux Densities

Flux densities of all sources were determined through integration over the source brightnesses determined by standard imaging/deconvolution algorithms. As shown in PB14, this straightforward method provides flux-density values equal in reliability to those provided by other methods. Atmospheric and instrumental phase fluctuations were corrected using phase self-calibration. Amplitude self-calibration was used to identify and to remove gain fluctuations in excess of ∼5%.[5] At the higher frequencies, nearly all of these are caused by small pointing offsets, while at the low frequencies, these are due to instrumental gain variations, which would likely have been corrected had we been able to utilize the switched power. Typically, 10%–20% of the data were removed by this process, with the fraction rising with frequency.

For many of the extended sources, correction of the image for attenuation by the primary beam is necessary. This was done for all cases where the correction is more than 0.5% using the recently determined primary beam coefficients (Perley 2016). We believe the correction is accurate to ∼1% when the attenuation is less than 10%.

3.2. Placing the Scale on an Absolute Standard

The process described above places the flux densities on a scale set by that assumed for the primary calibrator sources. For frequencies above 2 GHz, we have utilized the PB14 values for 3C286, 3C295, and 3C196, whose values are directly linked to absolute measurements of the planet Mars by *WMAP*, and which were shown by PB14 to be stable to better than 1% over the past 20 years. For frequencies below 2 GHz, we have used the Baars77 values for 3C405, whose values were determined via absolutely calibrated antennas, as reported in that paper. The choice of 2 GHz for the separation between these two standards was driven by two considerations.

1. The Mars-based calibration reported by PB14 has much higher errors below 2 GHz due to the weakness of Mars at these frequencies. Consequently, the PB14 values are much less secure below 2 GHz.
2. In the determination of the polynomial fits (described below) the residuals were significantly reduced for the three L-band frequencies when the Cygnus-A based values were utilized, compared to the Mars-based values.

3.3. Choice of 3C405 as the Absolute Standard below 2GHz

As noted, Baars77 provided "absolute" spectra for three sources, Cassiopeia A, Taurus A, and Cygnus A, and a "semi-absolute" spectrum for Virgo A.[6] Of these four, only Cygnus A provides a useable standard for absolute calibration by interferometers. The reasons are as follows.

[5] To prevent bias, the corrections were not applied to the data.

[6] Baars77 explains that this means its spectrum was determined directly through ratios to the three "absolutely absolute" sources.

Table 6
Fitted Coefficients for the 20 Sources

Source	a_0	a_1	a_2	a_3	a_4	a_5	χ^2	Freq. Range[a]
J0133–3629	1.0440	−0.6619	−0.2252	⋯	⋯	⋯	267	0.2–4
3C48	1.3253	−0.7553	−0.1914	0.0498	⋯	⋯	3.1	0.05–50
Fornax A	2.2175	−0.6606	⋯	⋯	⋯	⋯	17	0.2–0.5
3C123	1.8017	−0.7884	−0.1035	−0.0248	0.0090	⋯	1.9	0.05–50
J0444–2809	0.9710	−0.8938	−0.1176	⋯	⋯	⋯	3.3	0.2–2.0
3C138	1.0088	−0.4981	−0.1552	−0.0102	0.0223	⋯	1.5	0.2–50
Pictor A	1.9380	−0.7470	−0.0739	⋯	⋯	⋯	8.1	0.2–4.0
Taurus A	2.9516	−0.2173	−0.0473	−0.0674	⋯	⋯	1.9	0.05–4.0
3C147	1.4516	−0.6961	−0.2007	0.0640	−0.0464	0.0289	2.2	0.05–50
3C196	1.2872	−0.8530	−0.1534	−0.0200	0.0201	⋯	1.6	0.050–50
Hydra A	1.7795	−0.9176	−0.0843	−0.0139	0.0295	⋯	3.5	0.050–12
Virgo A	2.4466	−0.8116	−0.0483	⋯	⋯	⋯	2.0	0.05–3
3C286	1.2481	−0.4507	−0.1798	0.0357	⋯	⋯	1.9	0.05–50
3C295	1.4701	−0.7658	−0.2780	−0.0347	0.0399	⋯	1.6	0.05–50
Hercules A	1.8298	−1.0247	−0.0951	⋯	⋯	⋯	2.3	0.2–12
3C353	1.8627	−0.6938	−0.0998	−0.0732	⋯	⋯	2.2	0.2–4
3C380	1.2320	−0.7909	0.0947	0.0976	−0.1794	−0.1566	2.9	0.05–50
Cygnus A	3.3498	−1.0022	−0.2246	0.0227	0.0425	⋯	1.9	0.05–12
3C444	1.1064	−1.0052	−0.0750	−0.0767	⋯	⋯	5.7	0.2–12
Cassiopeia A	3.3584	−0.7518	−0.0347	−0.0705	⋯	⋯	2.1	0.2–4

Note.
[a] The frequency range, in GHz, over which the coefficients are valid.

1. Cassiopeia A and Taurus A are both supernova remnants, whose flux densities are expected to vary in time. Baars77 shows that this secular decrease for Cassiopeia A was typically 1% per year, and likely different at different frequencies. Although little is known of the variability of Taurus A, we show below that its flux density is also significantly decreasing over time. By contrast, Cygnus A is an extragalactic radio source, whose only sub-parsec component (the nucleus) capable of varying on timescales of interest comprises less than 0.1% of the total flux density at the frequencies of interest.
2. At 2 arcmin, Cygnus A is small enough to be usefully employed by interferometers. Furthermore, the hotspots of Cygnus are very compact (arcseconds) and very bright, leading to easily measured visibilities on long baselines. By contrast, the angular extents of Taurus A and Casseopeia A are 9.0 and 8.0 arcmin, respectively, while their compact components provide a very small fraction of the total flux. Although Virgo A contains significant compact structure, its angular size of 16 arcmin is much too large to be useful for calibration purposes for most interferometers.

The spectral flux densities derived from the process described above, and used in the subsequent polynomial fitting, are given in Table 5.

4. Polynomial Expressions for the Flux Densities

The frequency dependency of the spectral flux density for each source was obtained by fitting the data (via SVD) with a polynomial function of the form

$$\log(S) = a_0 + a_1 \log(\nu_G) + a_2 [\log(\nu_G)]^2 + a_3 [\log(\nu_G)]^3 + \cdots \quad (1)$$

where S is the spectral flux density in Jy, and ν_G is the frequency in GHz. With this formalism, a_0 is the log of the flux density at 1 GHz, and a_1 is the spectral slope at 1 GHz. Fits were made for linear (two terms) up to quintic (six terms) order polynomials, and the residual chi-squared examined for each of the fits. For all of the sources, the residual chi-squared drops steeply as more coefficients are added, but then flattens off after some number of terms. Since adding more coefficients for a slightly smaller reduced chi-squared has no physical basis, we utilize the number of coefficients at the point where the reduced chi-squared flattens. Since all of these sources are emitting via the synchrotron process, there is a strong preference to utilize the smoothest spectrum consistent with the data, which amounts to the minimization of the number of employed terms.

The resulting coefficients for all of the sources are given in Table 6. The fits for J0133–3629 and Fornax A are not considered reliable because these sources are too extended to permit reliable deconvolution with the limited data taken in this program. Note also that 3C48, 3C138, 3C147, and 3C380 are all known or suspected variable sources, with timescales for significant variations of a few years. Additionally, Taurus A and Cassiopeia A are SNRs with slowly decreasing flux densities. Their characteristics are discussed later in this paper.

5. Estimated Errors

5.1. Errors in the Measured Data Values

The errors in the determined spectral flux densities induced by the transfer process were derived with a method different than that utilized for PB14. For that paper, PB14 estimated the errors for each flux-density value by deriving the variance in the ∼10 individual observations whose average was used for the fit. This procedure is well justified for objects that are unresolved, or only slightly extended, as in this case, each

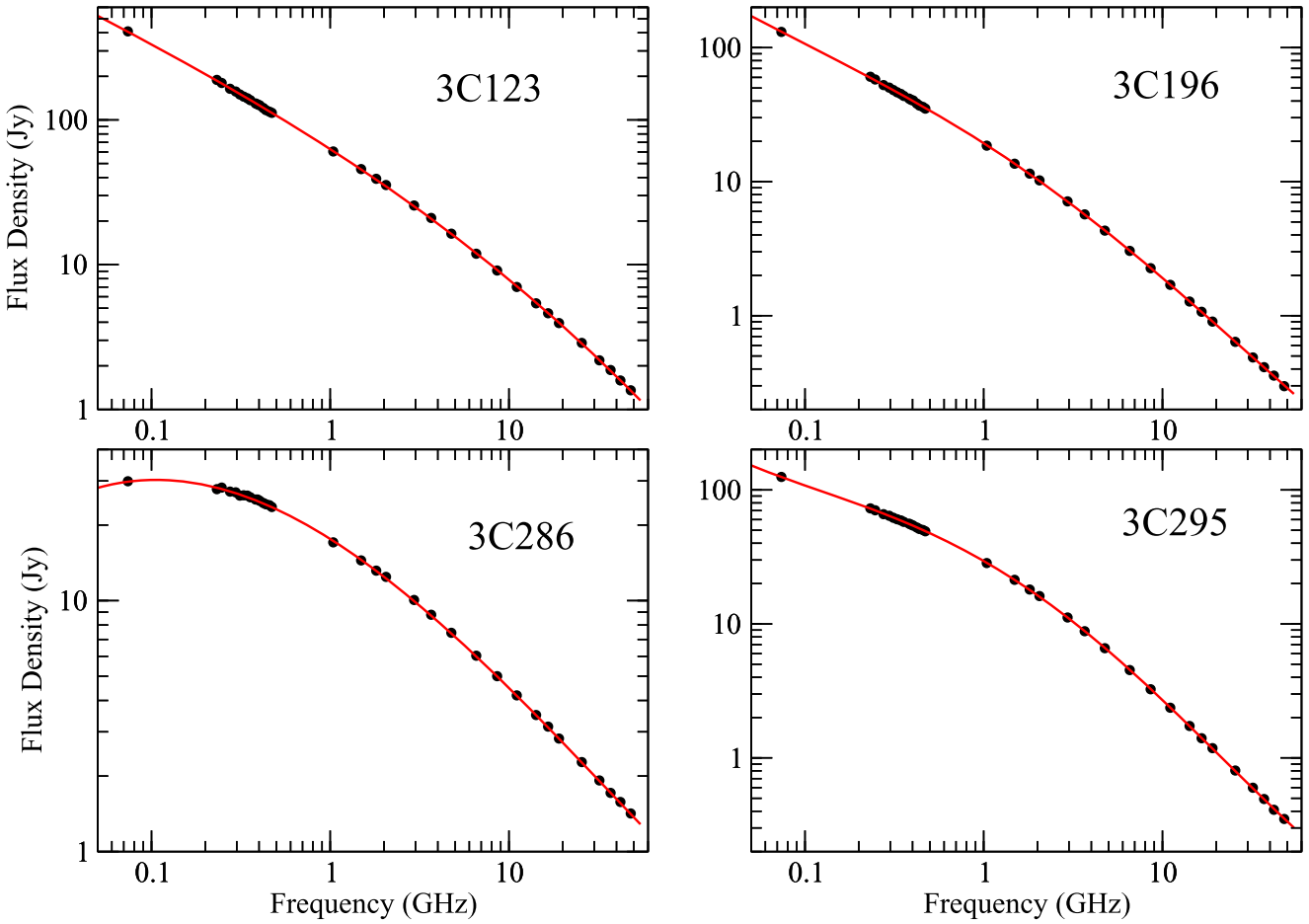

Figure 1. Plotted are the measurements of the flux densities of the four identified stable standards, and the best-fit models for each. For all values, the estimated errors are smaller than the plotted points.

Table 7
Ratio of This Scale to the PB14 Scale

Source	328 MHz	1488 MHz	2948 MHz	4764 MHz	8592 MHz	14192 MHz	19064 MHz	32064 MHz	42064 MHz
3C123	0.985	0.987	1.007	1.006	1.004	1.005	1.010	1.002	0.998
3C196	0.989	0.983	1.001	0.999	1.001	1.001	1.002	1.003	1.019
3C286	0.975	0.984	1.003	1.002	1.000	0.998	0.997	0.999	1.005
3C295	1.006	0.973	0.998	1.000	1.000	1.000	1.001	1.002	0.978

Note. Note that the PB14 scale is defined between 1 and 50 GHz. The ratios shown at 328 MHz are only to illustrate how close that scale comes to the new. The 1.8% offset noted at 1488 MHz reflects the transfer of the absolute standard from the Mars-based to the Cygnus A based absolute reference.

"snapshot" observation provides an independent valid estimate for the flux density. However, for highly extended sources—such as many of those included in this study—individual snapshots do not contain enough visibility data to enable a valid estimate of the flux density.

We have thus adopted an alternate approach that relies on the expectation that the spectra are smooth, and that the errors are multiplicative—i.e., they are proportional to the flux density of the source. The first criterion is well justified on physical grounds because the emission mechanism for all of these sources is synchrotron, which emits a broad, featureless spectrum extending over many orders of magnitude (Pacholczyk 1970). The second criterion is reasonable for the sources in our list, as the SNR for each source is such that additive (thermal) noise is far less than the scatter in the spectral fits. Thus, the effects of gain errors (whether they are due to receiver gain fluctuations or pointing errors) will scale with the source flux.

We have thus estimated the error by computing the variance in the ratio of the observed data values to the values predicted from the polynomial fits for all 20 sources for each of the 34 frequencies. The results show that, except for three of these 34 frequencies, the 1σ standard deviation is less than 0.8%. The three frequencies, which have notably higher errors, are 232 MHz (1.6%), 247 MHz (1.0%), and 48 GHz (4.7%). All three come from spectral windows known to be more poorly behaved than the others. At 48 GHz, the variation is due to poor SNR and poor pointing. At the two lower frequencies, the high residuals are due to the poor sensitivity at the low end of this band, combined with the flagging needed to remove the

Table 8
Ratio of This Scale to the SH12 Scale

Source	73.8 MHz	328 MHz
3C48	0.948	1.005
3C147	1.095	1.020
3C196	0.981	1.020
3C286	0.955	1.091
3C295	1.005	1.037
3C380	0.950	0.983

Note. The SH12 scale is defined between 30 and 300 MHz.

RFI. We believe our procedure for estimating the errors is as valid at 73.8 MHz as it is for the other frequencies. Independent data from both the A and B configurations were included—these gave completely consistent results—and, although the SNR is not as high as at the higher frequencies, the basic assumption that the errors are proportional to the source flux density is true, since all sources observed at 73.8 MHz are strong, and since the examination of the results shows no dependency of the scatter on spectral flux density.

These variances were used in estimating the coefficients, their errors, and the χ^2 of the polynomial fits. The coefficient errors, and their convariances, have not been included in Table 6 because the error in the proposed scale is dominated by that of the primary standard, Cygnus A, as discussed in the next section.

5.2. Flux Density Scale Errors

The remarkably good fits of simple polynomials to the data for all sources strongly indicate that the effect of instrumental transfer errors in the calibration and imaging process are much less than 1%, except at the highest frequency. Thus, we believe that the error in the proposed flux-density scale is completely dominated by the errors in the absolute standards—Cygnus A for frequencies below 2 GHz, and in the Mars-based flux densities above 2 GHz.

According to Baars77, the estimated error in the spectrum of Cygnus A, between 50 MHz and 2 GHz, is ∼2%–4%. PB14 estimated the accuracy of their scale to be 1%–3%, although a comparison of VLA and ATCA interferometric observations with Planck observations of 65 compact sources at 22 and 43 GHz by Partridge et al. (2016) suggests that the PB14 scale is low by ∼2.5% at 28 GHz, and by ∼5.5% at 43 GHz. We thus estimate the accuracy of our new, comprehensive scale, to be in the range of 3%–5%, with the larger errors at the lowest and highest ends.

The new data, and the new fits, for the four sources identified as constant to better than 1% over 20 years are shown in Figure 1.

6. Comparisons of This with Other Scales

Here we compare the values of our proposed new scale (herafter, referred to as the PB17 scale) with those given by the Baars77, SH12, and PB14 scales for selected frequencies.

6.1. Perley & Butler (PB14)

Table 7 shows the ratio of PB17 scale values to the PB14 scale, utilizing the four established stable sources.

Table 9
Ratio of This Scale to the Baars77 Scale

Source	328 MHz	1488 MHz	2948 MHz	4764 MHz	8592 MHz	14192 MHz
3C48	0.978	1.025	1.017	1.006	1.009	1.036
3C123	1.074	0.991	0.973	0.948	0.925	0.910
3C144	0.777	0.888	0.904	…	…	…
3C147	1.010	0.993	0.967	0.951	0.964	1.022
3C218	0.999	1.027	0.970	0.933	0.886*	
3C274	0.907	1.000	…	…	…	…
3C286	0.977	1.013	1.004	0.987	0.976	0.979
3C295	1.001	1.012	0.999	0.980	0.974	0.997
3C348	0.969	1.057	1.038	0.994	0.925*	
3C353	1.034	1.007	1.038	…	…	…
3C405	1.000	1.006	0.975	0.977	1.009	
3C461	0.820	0.846	0.821	…	…	…

Note. Shown are ratios where both the Baars77 scale is defined and for which we have data. Values marked with an asterisk are known to be too low, due to over resolution by the VLA.

There is excellent agreement between the PB14 and PB17 scales. This is expected because the four sources are known to be time-invariant over periods much longer than the time between these measurements. The average deviation of 0.982 for the 1488 MHz value reflects the change in absolute standard, from the (poor SNR) value based on Mars in PB14, to the Cygnus A standard adopted here.

6.2. Scaife & Heald (SH12)

Table 8 shows the ratios of the PB17 scale values to the SH12 scale values.

The SH12 scale is shown to be quite close to the absolute, with only 3C286 showing more than ∼5% discrepancy. This might be due to the presence of unusually close confusing sources. The low value in the flux density for 3C380 can be attributed to its known variability; see the discussion below.

6.3. Baars et al. (Baars77)

Table 9 shows the ratio of the PB17 scale to that of Baars77.

There is, in general, good agreement between the scales for those frequencies where the more extended sources are not heavily resolved by the VLA observations. The much lower values for 3C144 and 3C461 reflect the decline in the flux density of these two supernova remnants over time. The variations for 3C48 and 3C147 can be attributed to these sources' known slow variability. The drop in flux density for 3C123 is more surprising—this is discussed below.

7. Comments on the Sources

Here we present short summaries of each of the target sources, with emphasis on the suitability of each for radio telescope calibration purposes.

7.1. 3C123

This source, a radio galaxy at redshift $z = 0.218$, is one of the unchanging sources identified by PB14. Its angular size of 44 arcsec makes it of limited use for high-resolution interferometers. See PB14 for an image with 3 arcsec resolution. Roughly speaking, it is too heavily resolved on baselines exceeding 200 Kλ to be used as a calibrator. In VLA terms, this

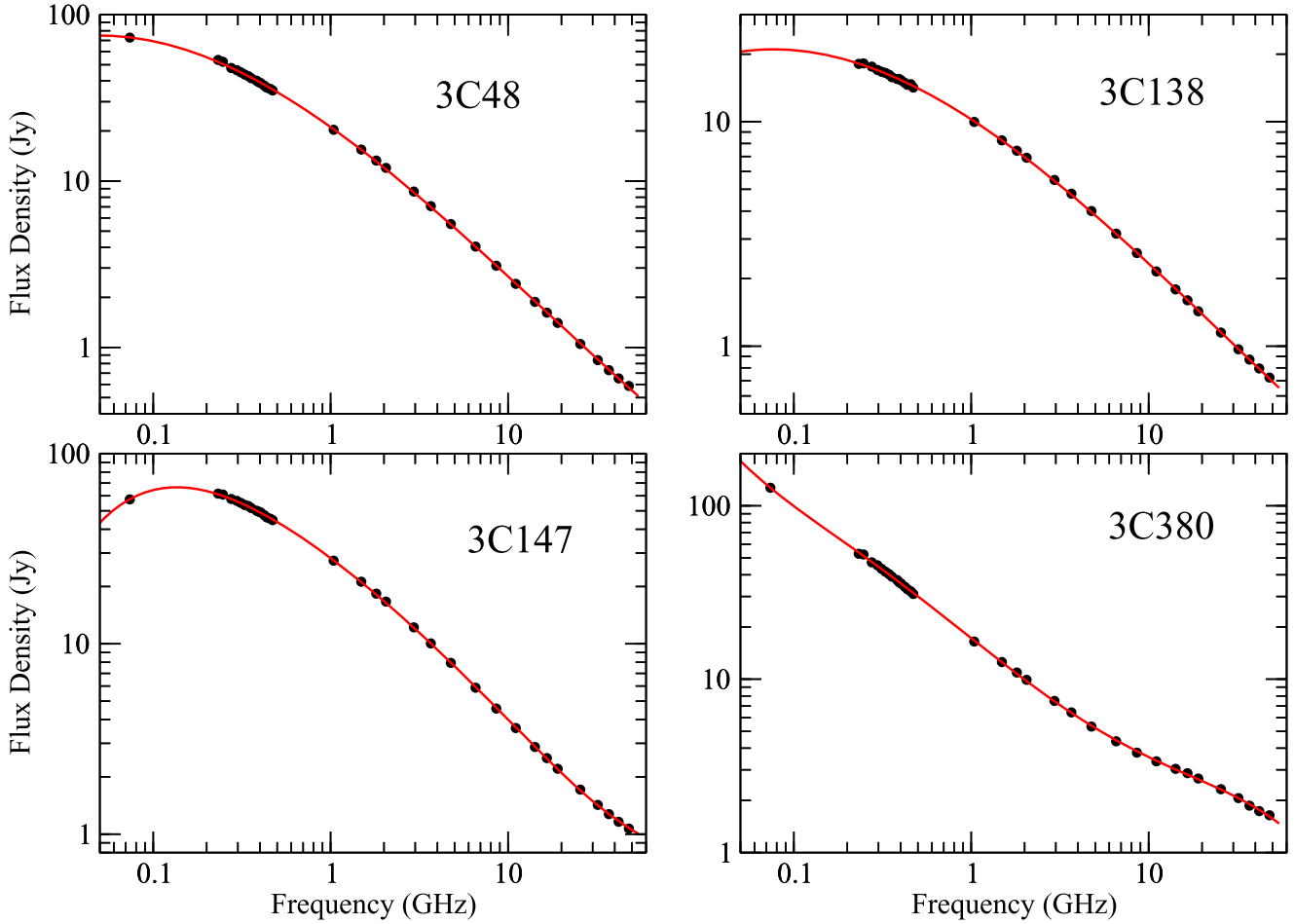

Figure 2. Showing the spectra and fits for 3C48, 3C138, 3C147, and 3C380. Errors are smaller than the plotted points. The inflection in the spectrum for 3C380 seen at the highest frequencies is due to the strong, flat-spectrum nuclear emission.

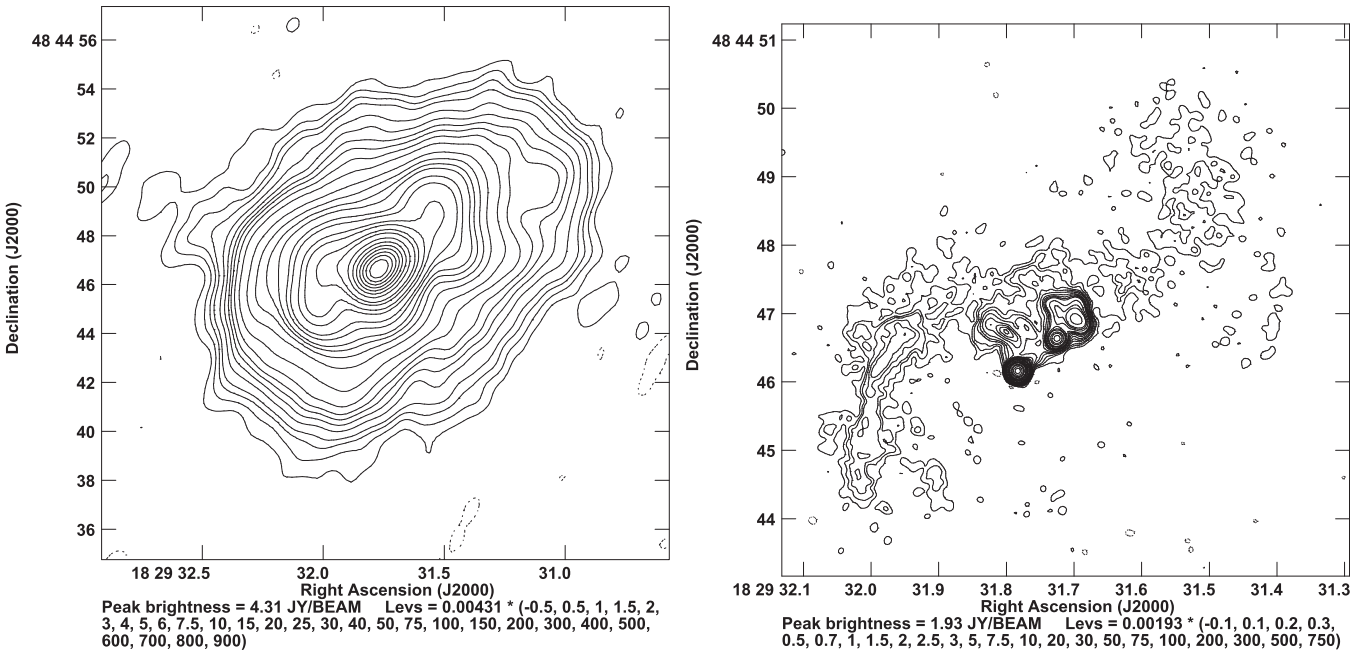

Figure 3. Images of 3C380. (Left) The structure at 1488 MHz with 1.4 arcsec resolution. The smooth elliptically shaped halo has dimensions of 16 × 12 arcsec. (Right) The structure at 16564 MHz with 0.125 arcsec resolution cannot detect the halo, and is dominated by a complex of very compact features. The more northern of the two compact features is the nucleus.

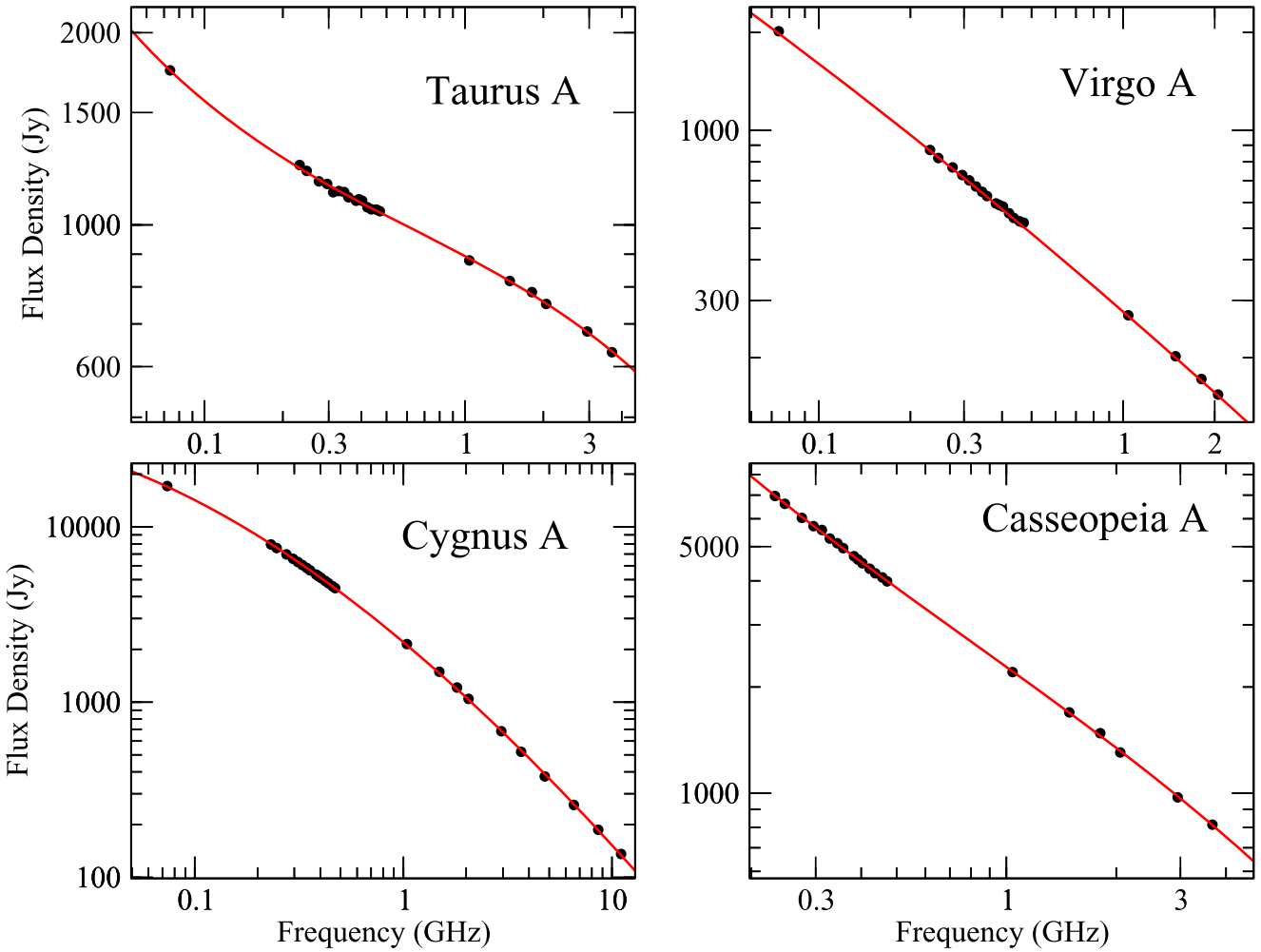

Figure 4. Spectra and fits for the four Baars77 "absolute" standard sources. The plotted values for Taurus A and Casseopeia A—both variable sources—are from 2016.

corresponds to frequencies above 2 GHz, though it could be used in the compact C and D configurations up to 12 GHz.

The new data show no evidence of any secular change (to ∼1%) in flux density since 2012. However, comparison (from Table 9) to the PB14 scale shows that current flux density is now considerably lower than that given in Baars77, from 1% at 1488 MHz to 9% at 14.2 GHz. It is very unlikely that the Baars77 scale could be this much in error, and we suggest that the nucleus of the source is now much less strong than it was prior to 1975. If real, the decline is significant because the nuclear emission flux density is currently about 100 mJy from 1.5 through 15 GHz, a drop of about 400 mJy from the levels needed to reconcile these measurements to the scale of Baars77. However, this hypothesis is unlikely to explain the 7% rise in the flux density at 328 MHz—though it should be kept in mind that the Baars77 scale is not valid at that frequency.

7.2. 3C196

This source, a quasar at redshift $z = 0.871$ is a ∼7 arcsec double with compact lobes. The structure is shown in PB14. Table 7 shows no change in flux density to an accuracy of better than 1%. The nuclear core is extremely weak—less than ∼2 mJy at all frequencies. The lobe structures, though compact, are of kiloparsec scale, ensuring no significant change in flux density on long timescales. The small size, high flux density and simple spectrum make this source an excellent calibrator at low frequencies.

7.3. 3C286

This extraordinary source, a quasar at redshift $z = 0.846$ is very compact, with weak, steep-spectrum structures extending about 3 arcsec to the west, and 0.5 arcsec to the east of the nuclear core, as shown in PB14. The absence of any detectable variabililty in both the total flux density and polarized emission is likely linked to the absence of an inverted spectrum core—a most unusual, and perhaps unique—feature for such a compact object.

7.4. 3C295

This is a radio galaxy at redshift $z = 0.464$, with a simple double-lobed structure of angular size 5 arcsec, and a weak nuclear core of about 5 mJy. There is no sign of variability in the spectral flux density. This is as expected because the nuclear emission at all frequencies is less than 1% of the total.

7.5. 3C48

This source, a compact (1.2 arcsec maximum extent) steep-spectrum quasar of redshift $z = 0.367$ was shown to be slowly

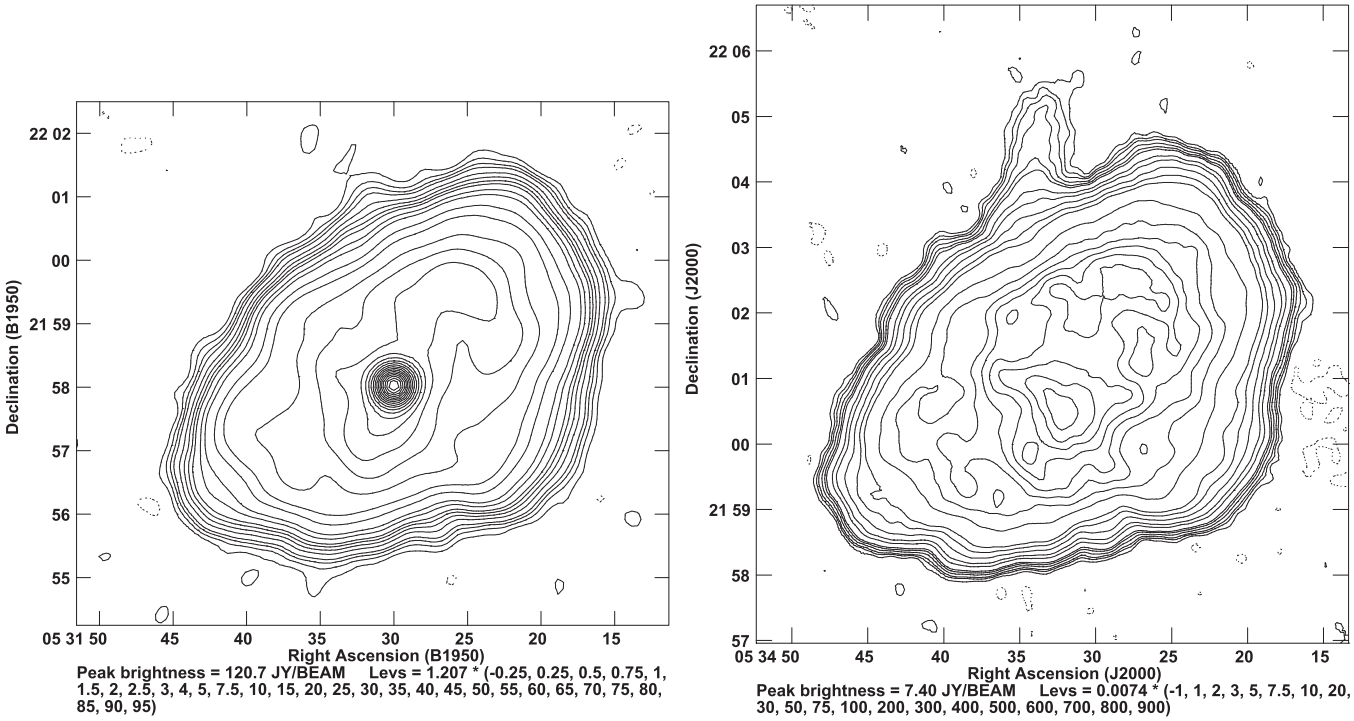

Figure 5. Taurus A (Crab Nebula, 3C144) at 73.8 MHz with 30 arcsec resolution (left), and at 1488 MHz with 17 arcsec resolution (right). The major difference is the pulsar, whose averaged 73.8 MHz emission of 90 Jy is easily visible in the left panel, but is not perceptible at 1488 MHz. The plume, which is easily visible at 1040 MHz, is at the noise level in the 73.8 MHz image.

variable in PB14. Its structure is shown in PB14. Comprison of the current values to those of PB14 show no change exceeding 2% between 1 and 50 GHz. Its spectrum is shown in Figure 2.

7.6. 3C138

PB14 showed that this source—a Compact Steep Spectrum (CSS) quasar of redshift $z = 0.759$ with maximum extent ∼0.7 arcsec has undergone a significant flare from its nuclear core, starting in 2002, peaking in 2010, and declining therafter. The new observations show the flux density continuing to decline over all frequencies, with current (2016) values some 5%–16% lower than in 2012. Because of these significant variations, this source is not recommended as a flux-density calibrator, although its high polarization appears to be rather more stable. Its spectrum is shown in Figure 2, and its structure in PB14.

7.7. 3C147

PB14 showed that this source has had sporadic flux density changes from its nuclear core of up to 20% on short (few years) timescales over the period of 1980 through 2012. The recent data show a sudden increase in flux density at the highest frequencies—from barely 1% at 2 GHz to over 20% at 48 GHz. Because there is little change in flux density between our 2014 October and 2016 January observations, this increase must have occured between 2012 January and 2014 October. Its spectrum is shown in Figure 2 and its structure—with a maximum extent of ∼0.9 arcsec, is shown in PB14.

7.8. 3C380

This source, a CSS quasar at redshift $z = 0.691$ was included in the new observations since it is included in the list of SH12. It has a complex structure, showing both a diffuse elliptical halo, and a central complex, comprising a number of very compact sources, including a strong, unresolved nucleus, as shown in Figure 3. The central highest-brightness feature is the flat-spectrum nucleus. Its overall source spectrum (for 2016) is shown in Figure 2. The emission at higher frequencies is increasingly dominated by the flat-spectrum nucleus. VLBA observations of this component by Lister et al. (2013) show a highly superluminal jet ($\beta \sim 13.1$) emanating to the NW from the core. As expected by the presence of a strong core and milliarcsecond jet, this source is highly variable—the 2016 January data show the flux density to have declined from the 2014 October value by ∼3% at 16.6 GHz to nearly 30% at 48 GHz. Because of this, and the size and complexity of the structure, this object is only of value for calibration at the lowest frequencies, where the variability is much reduced, and the angular scale of the halo is not of concern.

7.9. Taurus A

The spectrum of this famous source is shown in Figure 4. Taurus A is an SNR and a pulsar wind nebula resulting from a bright supernova in the year 1054 AD. The central pulsar is powering the synchrotron emission, and the radio-emitting nebula is expanding outward at about 0.15 arcsec yr^{-1} (Beitenholz et al. 1991). Low-resolution images of the source at 1488 and 73.8 MHz are shown in Figure 5. The observed expansion and presence of the pulsar strongly suggest that the source may be variable. We can find little information on any measured secular change of the flux density. However, the current flux density between 1 and 4 GHz is 10%–15% lower than the values given by Baars77. Because it is very improbable that the latter value will be in error by this much,

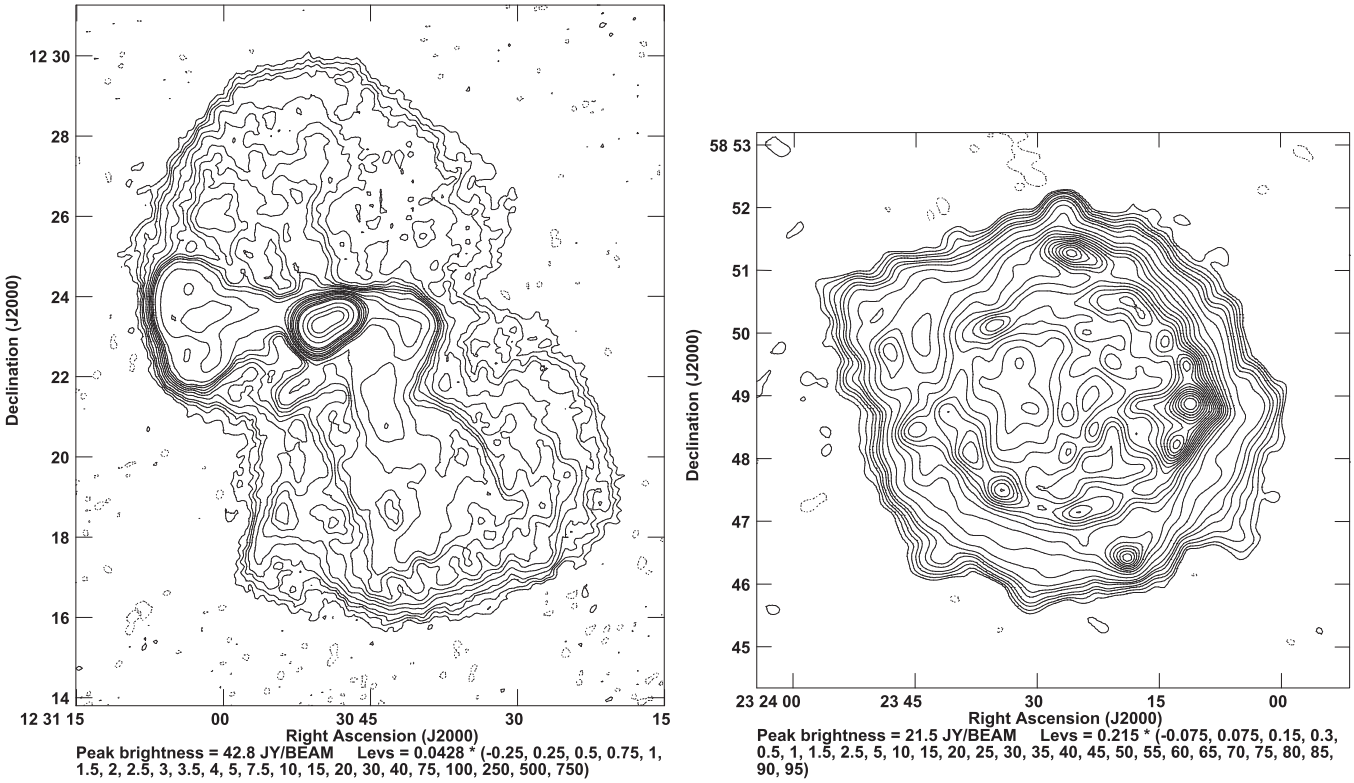

Figure 6. (Left) Virgo A at 1488 MHz, with 24 arcsec resolution. The compact region in the center contains the well studied one-sided jet. The diffuse lobes extend over 14 arcmin. (Right) Cassioepeia A at 1488 MHz, with 17 arcsec resolution.

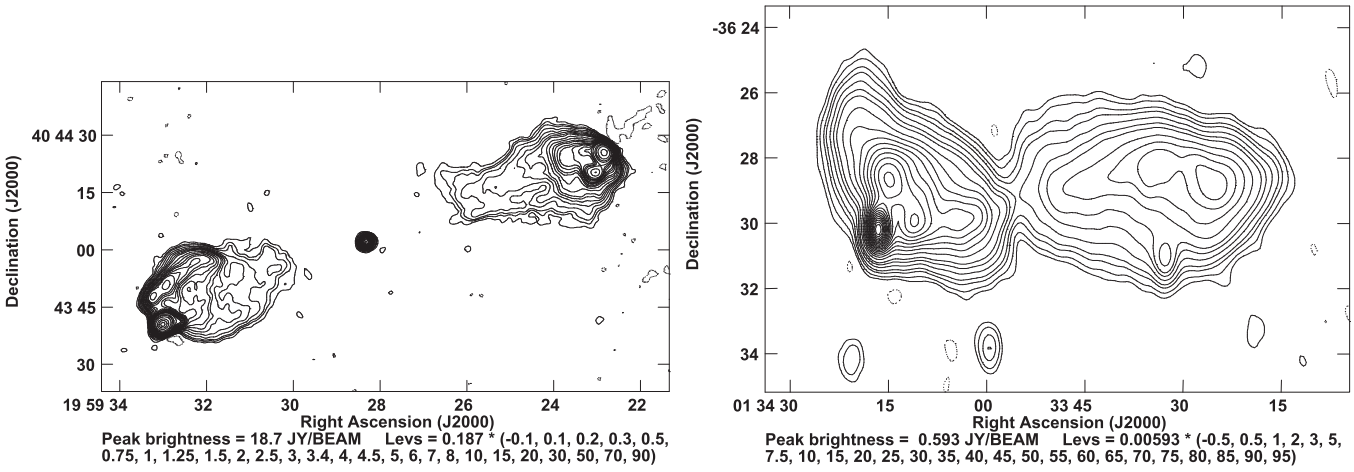

Figure 7. (Left) Cygnus A at 11.06 GHz, with 2.25 arcsec resolution. The source has a maximum extent of 130 arcsec, with bright and compact hotspots. (Right) The southern source J0133–3629, at 1.04 GHz with 60 × 30 arcsec resolution.

the indication is that the source's flux density is declining by approximately 0.25% per year.

The large extent, lack of small angular scale structure, and secular changes all argue that this source is unsuitable as a flux-density standard.

7.10. Virgo A

The radio emission from this well-known radio galaxy is very well studied thanks to its proximity (16 Mpc) and angular size (14 arcmin). Besides the one-sided jet, the source is comprised of very faint and extended radio lobes, as shown in Figure 6. It is the presence of these very large and diffuse structures that make this source very problematical for calibration purposes, except for low-resolution arrays and single-dishes. The current flux density from 1 to 4 GHz is within 1% of the Baars77 value. However, at the P band, the newly measured values are low by about 5% compared to Baars77. Its spectrum is shown in Figure 4.

7.11. Cassiopeia A

This very strong radio source is identified with an unseen SN approximately 300 years old. It has long been identified as the strongest extra-solar radio source. However, its continued secular decline has relegated it to second place, behind Cygnus

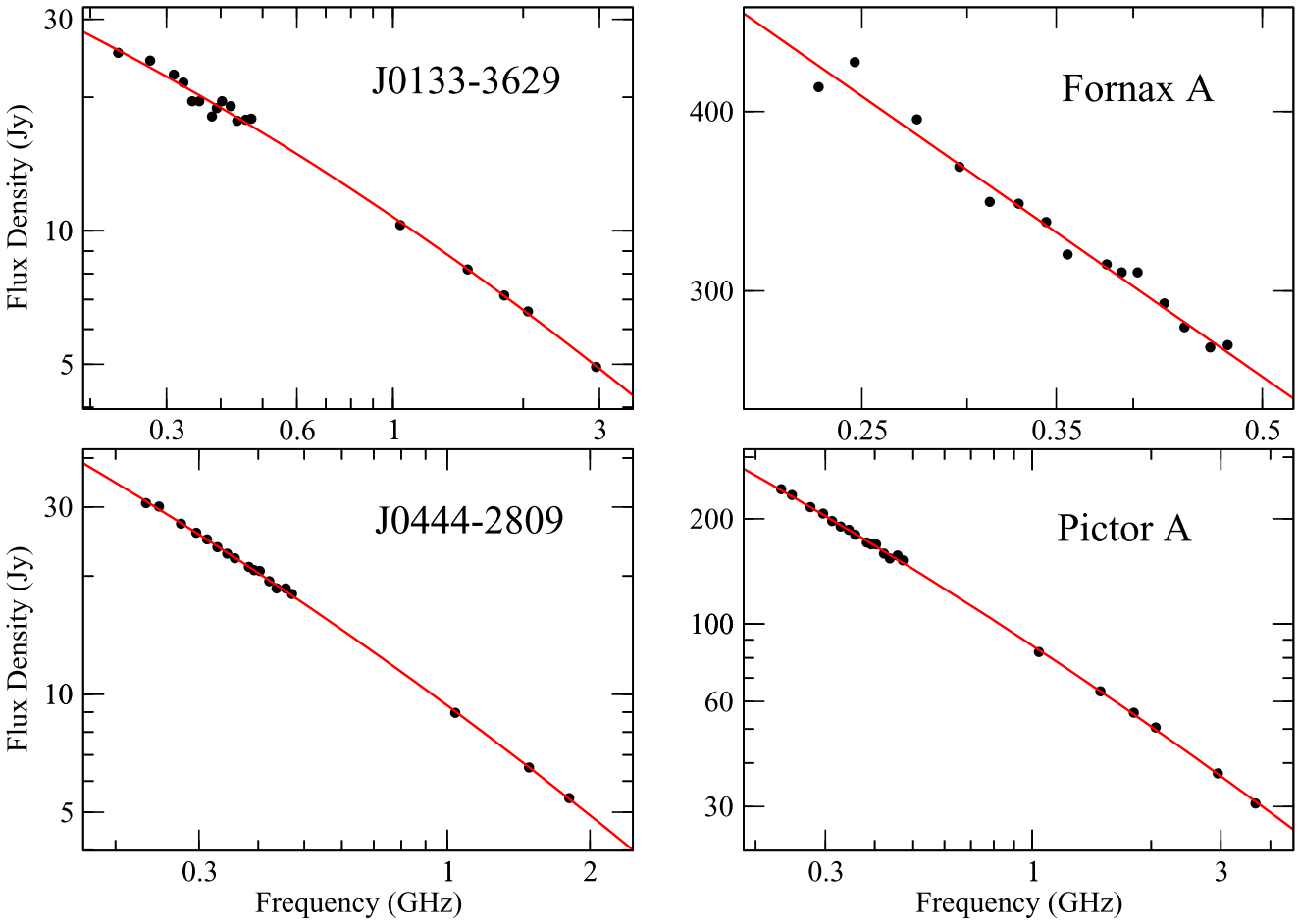

Figure 8. Spectra of four of the southern calibrators. The poor fits for J0133–3629 and Fornax A reflect the difficultly in accurately reconstructing large, far southern sources with just a few VLA snapshot observations.

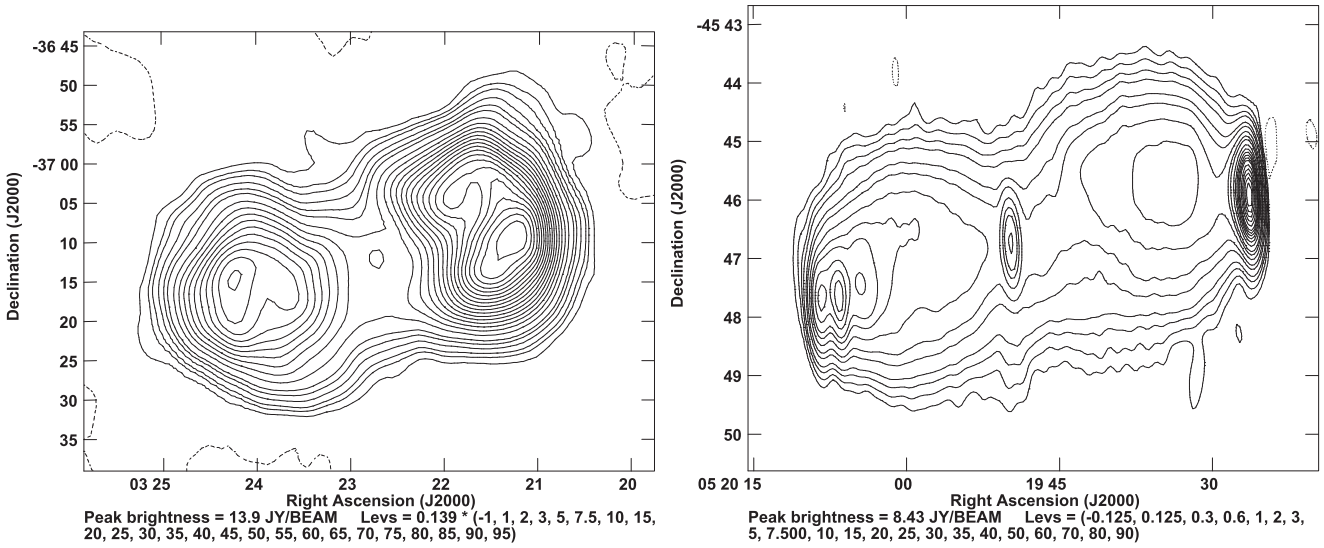

Figure 9. (Left) Fornax A at 312 MHz with 200 × 275 arcsec resolution. This object is too large to be properly imaged with only a few VLA snapshots. (Right) Pictor A at 1808 MHz and 14 × 65 arcsec resolution.

A, for frequencies below ∼1 GHz. The structure at 1488 MHz, with 17 arcsec resolution, is shown in Figure 6. Its spectrum (2016) is shown in Figure 4. Its large angular size, steady spectral flux-density decline, and generally diffuse structure make this a poor object for calibration purposes. The flux density is declining at a rate given by Baars77 as $-0.97 + 0.3\log(\nu_G)\%$ per year. However, our recent measurements indicate a much slower decline: the 74 MHz flux density measured in 1998 is down by 9% from the 1977 value—a 0.41% per year decline. The 2016 flux density, from 230

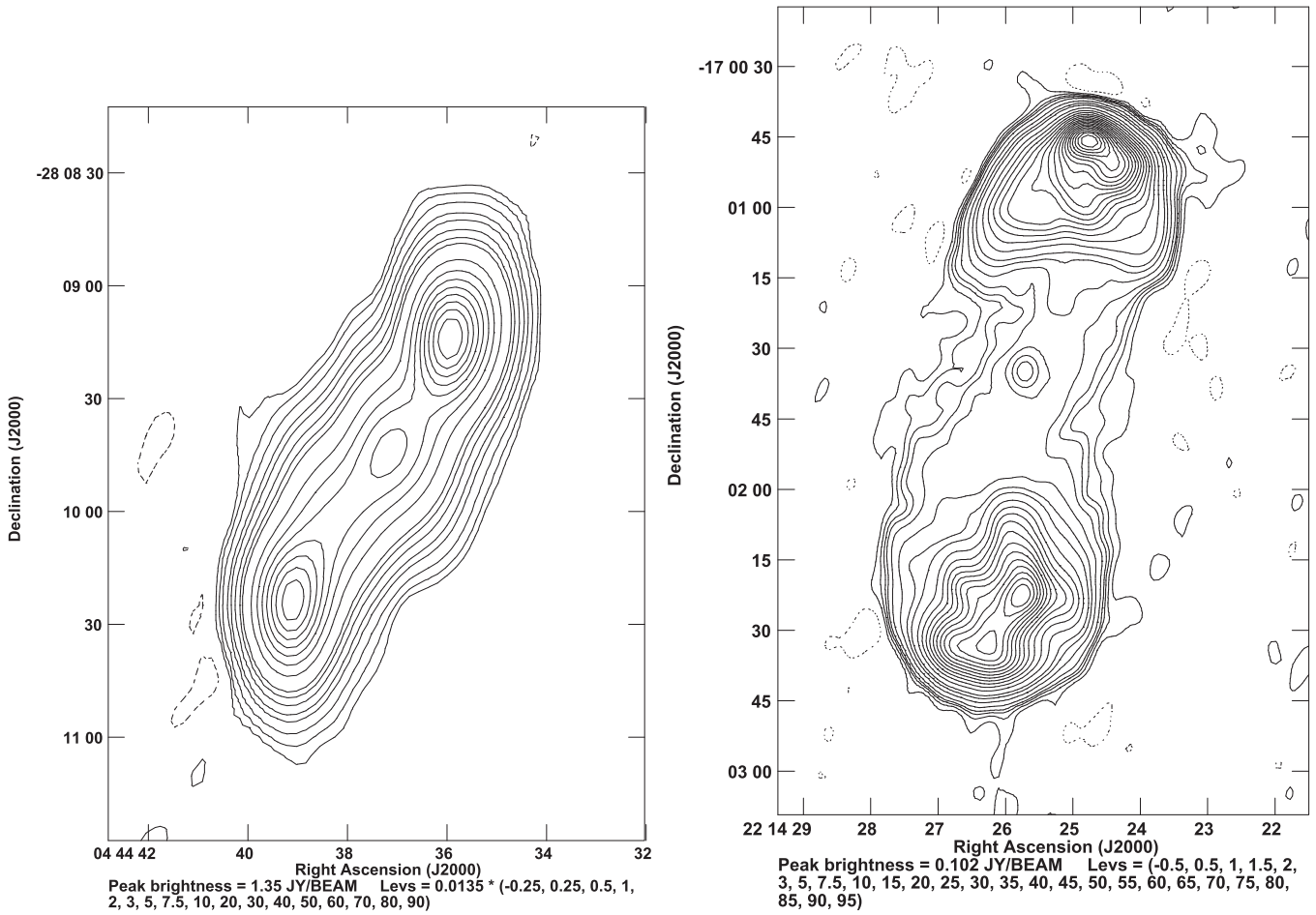

Figure 10. Images of J0444–2809 at 1808 MHz with 25 × 13 arcsec resolution, and 3C444, at 4764 MHz with 7 × 5 arcsec resolution.

through 4000 MHz is 18% lower than the Baars77 value for 1977—a 0.46% per year decrease.

7.12. Cygnus A

Cygnus A (3C405) is a nearby ($z = 0.056$) luminous radio galaxy. Due to its proximity and very high flux density, its structure has been extensively studied. An image at a frequency of 11 GHz with 2.25 arcsec resolution is shown in Figure 7. With a maximum extent of just 2 arcmin, and with very bright and sharp arcsecond-scale spatial features, the source is a good flux-density calibrator for objects at low frequencies to moderate-resolution arrays. Its spectrum is shown in Figure 4. Other than the 1 Jy nuclear source, the most compact features have physical extents of hundreds of parsecs, so that secular changes in flux density on decadal timescales must be at a very low fractional level.

The remaining eight objects are all southern sources, and were included in this study as an aid to transferring the northern calibrator network to the southern hemisphere.

7.13. J0133–3629

This source is a very large (14 arcmin) and diffuse double-lobed object with a bright compact hotspot in the eastern lobe. The nuclear emission from this source is weak (30 mJy at 2.9 GHz), so that measureable variability in the total flux density is unlikely. Nevertheless, this is a poor object for use by interferometers for flux-density calibration, due to its large size and diffuse structure. Its spectrum is shown in Figure 8.

7.14. Fornax A

This source, associated with the galaxy NGC 1316, is a nearby (19 Mpc) large (55 arcmin) and extremely diffuse radio galaxy. Its angular size is too large to enable the VLA to make accurate flux-density measurements above 1 GHz. The limited snapshot observations of this program are not sufficient to permit accurate reconstruction of its structure, so that the integrated flux densities, and the spectrum shown in Figure 8 must be viewed with considerable skepticism. Figure 9 shows a low-resolution image at 312 MHz, with 200 × 275 arcsec resolution. This source is too large and diffuse to be useful as a primary calibrator for high-resolution interferometers.

7.15. Pictor A

This FRII radio galaxy is a large (8.3 arcmin) and strong source. An image at 1808 MHz with 14 × 65 arcsec resolution is shown in Figure 9. Its spectrum is shown in Figure 8. The prominent hotspots make this a useful object for interferometric calibration. The compact nuclear source contributes less than 0.5% of the total flux density at the P band, so any secular variations of this component at that frequency will have a negligible effect on the total flux density. At higher frequencies, its large angular size and the increasingly

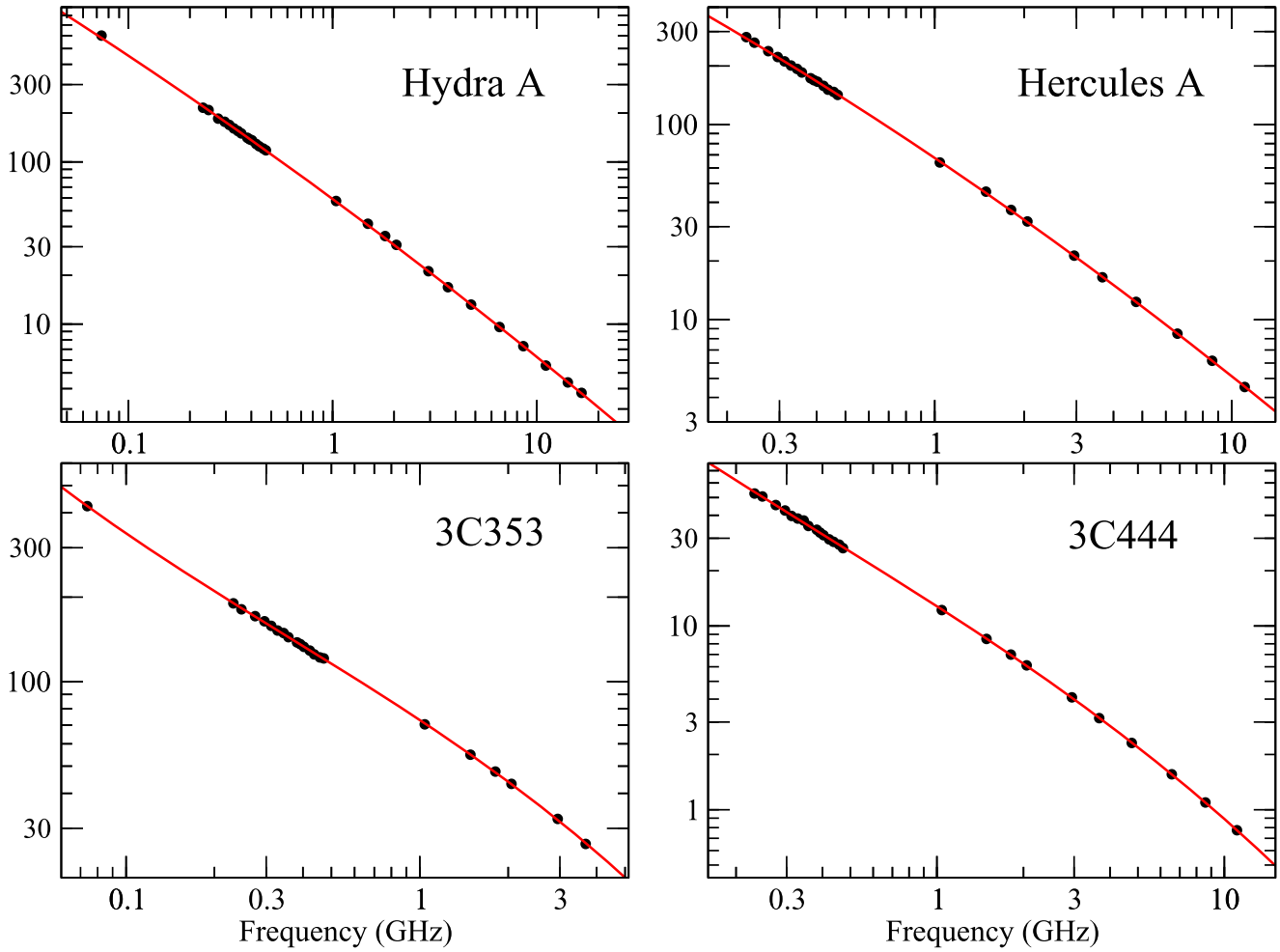

Figure 11. Observed data and LSQ fits for Hydra A, Hercules A, 3C353, and 3C444. Errors are smaller than the plotted points.

prominent nucleus make this source unsuitable for calibration purposes.

7.16. J0444–2809

This double-lobed radio source is relatively compact (2 arcmin) and strong, making it a potentially useful calibrator. A low-resolution image (25×13 arcsec) at 1808 MHz is shown in Figure 10. Its spectrum is shown in Figure 8. Due to a scheduling error, we did not observe this potentially useful calibrator at a higher frequency.

7.17. 3C444

An image of this $z = 0.153$ radio source, at 4764 MHz with 7×5 arcsec resolution is shown in Figure 10. Its spectrum is shown in Figure 11. Its maximum size of two arcminutes, and absence of a prominent core, make it a useful calibrator for low-frequency interferometers of moderate resolution.

7.18. Hydra A

Hydra A (3C218) is an FRI radio galaxy lying in the center of the Abell cluster A780. It has extensive, low-brightness large-scale structure, as well as compact jet and nuclear structure near the center. These features are illustrated in Figure 12. VLA images taken at 74 MHz by Lane et al. (2004) show the southern low-brightness emission extending much further to the east. The overall extent of about 8 arcmin, complexity of structure, and the relatively strong nuclear core make this a problematic object for flux-density scale calibration above 1 GHz. Its spectrum is shown in Figure 11.

7.19. Hercules A

Hercules A is a radio galaxy with redshift $z = 0.155$. Its structure at 6564 MHz with 5 arcsec resolution is shown in Figure 13. The maximum extent of 3.1 arcmin makes this a difficult object for calibration by high-resolution arrays, though its very weak nuclear emission strongly suggests that the source flux density will be very stable. Its spectrum is shown in Figure 11.

7.20. 3C353

3C353 is a nearby radio galaxy of redshift $z = 0.0304$. The radio structure is very large (5.3 arcmin), and quite complicated. An image at 2948 MHz, with 25×13 arcsec resolution, is shown in Figure 13. As the nuclear flux is very weak (less than 0.1 Jy, so much less than 0.1% of the total flux), the total flux density is expected to be very stable. Its spectrum is shown in Figure 11.

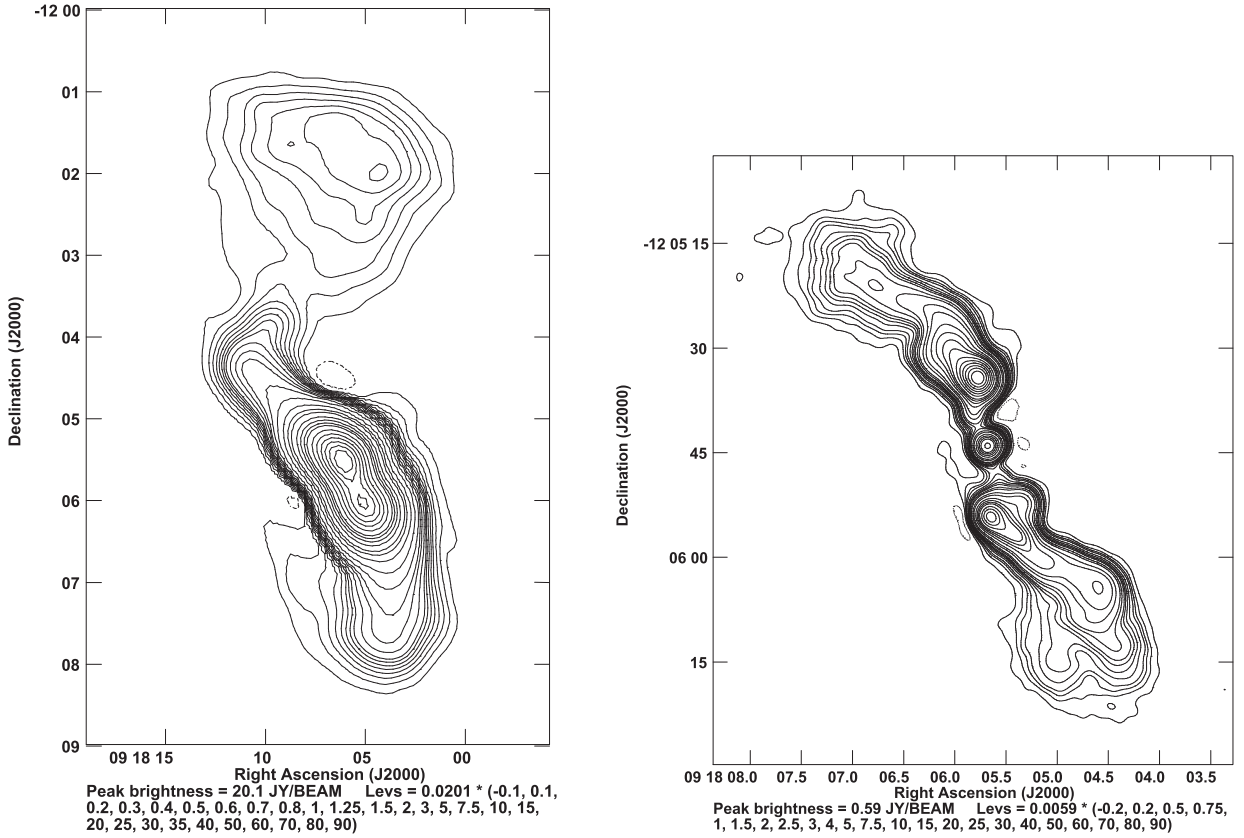

Figure 12. (Left) 3C218 at 1040 MHz with 28 arcsec resolution. (Right) The central regions of 3C218 at 11.06 GHz, with 2.65 arcsec resolution. At this frequency, the extended emission has faded below detectability.

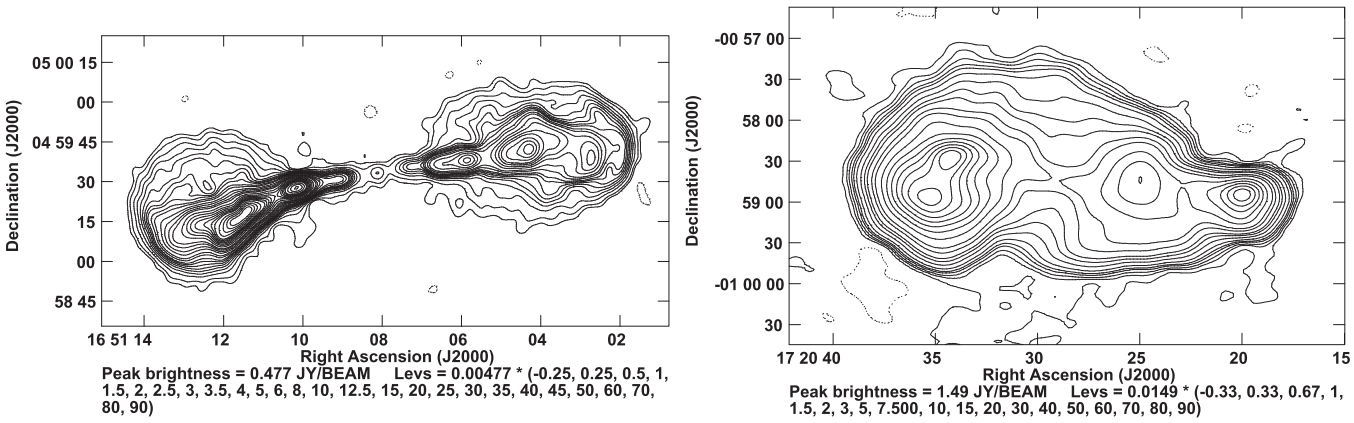

Figure 13. (Right) Hercules A at 6564 MHz with 5 arcsec resolution. (Left) 3C353 at 2948 MHz and 13 × 25 arcsec resolution.

8. Discussion

What is the best means for providing accurate gain calibration for an interometric array? In principle, accurate instrumental amplitude calibration can be done without the use of an external standard. As shown in PB14, what is required is a good knowledge of the antenna gain (or aperture efficiency) and of the on-board noise calibration power. The antenna efficiency is generally a function of antenna elevation and observing frequency, and will differ, possibly significantly, among the antennas of an array. It has generally been argued that the effort involved in measuring, monitoring, and implementing the necessary efficiency and calibration noise parameters for an array is not cost effective, and that external calibration schemes are sufficient. Additionally, it should be added that external factors, such as weather, are not accounted for with an internal-only calibration scheme.

Because of these issues, most arrays utilize an external flux-density standard source for amplitude gain calibration. Provided that antenna and system electronics gains do not change, or change in a known way between observations of the target and the standard gain calibrator, accurate gain calibration only requires the application of correlation ratios between the target and reference objects.

The question then becomes, what makes a good flux-density scale calibrator? It is easy to list the ideal properties—unresolved at all bands and baselines, unchanging on time-scales of decades and strong enough so that system noise and

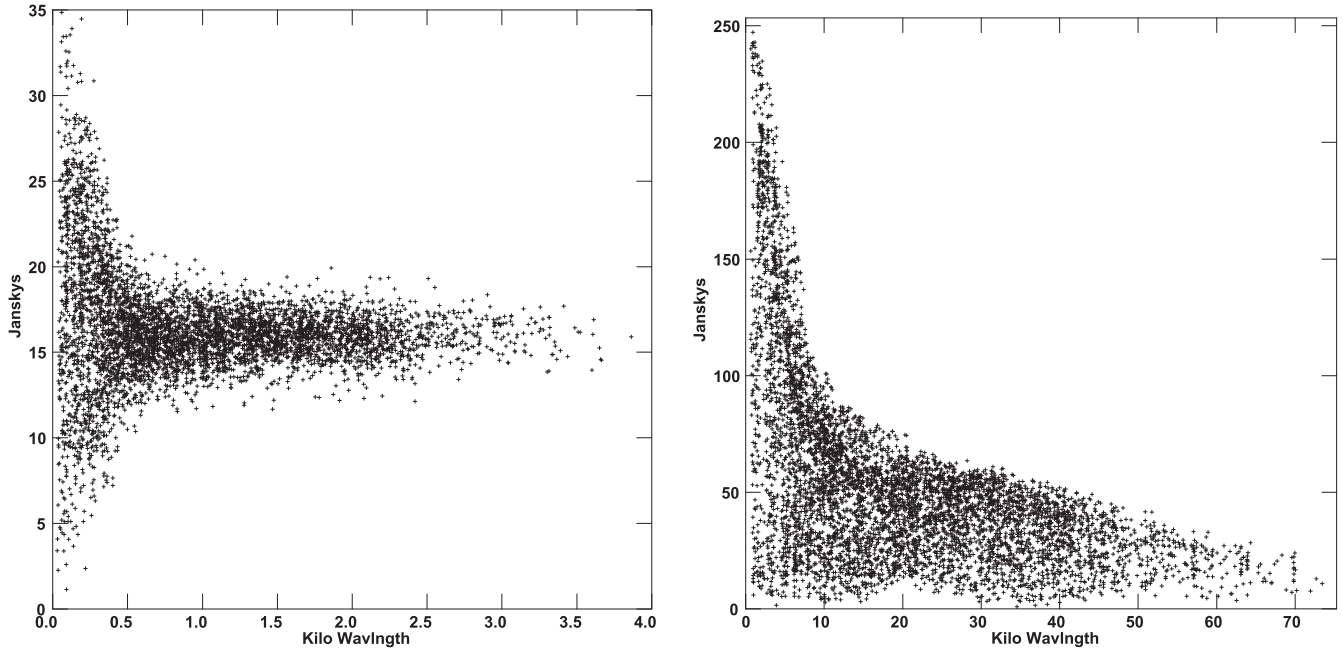

Figure 14. (Left) Visibility function of 3C138 at 344 MHz. The scatter in the visibility amplitudes is due to the Crab Nebula, located 6.°4 away. (Right) Cygnus A at 6564 MHz. The smooth lobes are resolved out at about a 10^4 wavelength baseline. The slow decline thereafter is from the gradual resolution of the bright hotspots.

background source confusion are negligible. There is no such source. It seems to be a law of nature that sources small enough to remain unresolved over a wide range of resolutions and frequencies are necessarily variable. Furthermore, the strongest stable sources are nearly all significantly resolved to modern high-resolution arrays.

Thus, we must utilize partially resolved objects for accurate amplitude gain calibration. What criteria should we apply when deciding which sources to utilize? These include the following.

1. Stable for long periods—preferably decades, but at least years. Less satisfactory, but potentially acceptable, is a known secular change. Although slowly variable objects can be monitored fairly easily, the overhead in doing so and disseminating results imposes significant additional costs and risks.
2. Small enough not to be resolved out by the longest spacings in a given array. Use of a partially resolved source model requires an accurate model as a function of frequency, but if the source is non-variable, there is no fundamental problem with this. Additionally, the object should be much smaller than the component antennas' primary beam, so that frequency-dependent corrections are not necessary.
3. Strong enough so the effects of confusion and system noise are neglible in the solution for the antenna gains. Confusion is an issue for lower frequencies, system sensitivity for higher frequencies.

We have reviewed the characteristics of the 20 sources included in this study, and generated criteria to judge the suitability of each for amplitude calibration by arrays of the scale of the VLA, over the 50 MHz–50 GHz span of this study. Specific criteria, and comments, are given below. We note that many of the criteria chosen are arbitrary, and many of the ranges given are specific to the VLA, and its 25 m primary antennas. It should be relatively straightforward to modify these for any given array.

1. *Stability:* The total flux density should not change by more than 2% per year, unless in a predictable way. For extended sources comprising a (presumably variable) nuclear core, if we assume that the core can change 40% in one year (a likely worst case), the nucleus flux must be less than 5% of the total.
2. *Angular Size:* The source should not be attenuated by the primary beam by more than 2%. This criterion is strongly frequency dependent, both because the primary beam size varies linearly with wavelength, and from spectral index gradients in the extended emissions of the sources.
3. *Resolution:* The visibility of the longest spacing should be at least 5% of the total, to ensure that a source model predicts enough visibility for stable gain solutions for the most distant antennas. Essentially, this requirement tries to limit the diffusiveness and complexity of the necessary source model. Furthermore, the visibility amplitude on the longest spacing must be at least 10 times the rms noise in the visibilities for the time and frequency averaging used in the solution. For the VLA, this translates to ∼100 mJy for the central bands (L through X), rising to 300–500 mJy at both low and high frequencies.
4. *Background Source Confusion:* Nearby confusing sources are effectively a source of noise in the gain calibration. Modeling these is difficult, since their effect on the visibilities will depend on the time and frequency averaging used in the calibration solution. To minimize gain solution variations, we require the confusion noise in the visibilities to be less than 50% of the total flux, and must resolve out before one-third of the maximum baseline.

The criterion regarding confusion might be considered too loose, but in fact the contributing background sources have random phases, such that the antenna-based gain solutions have remarkable isolation to their presence. In fact, they can be

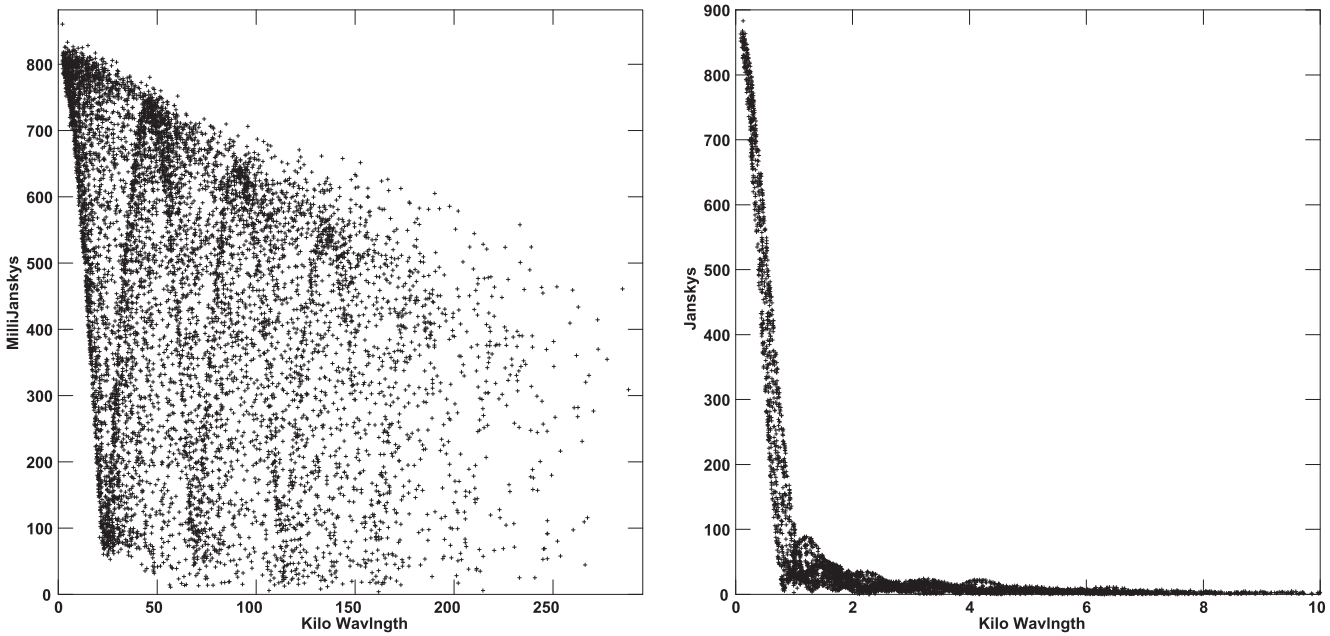

Figure 15. (Left) Visibility function of 3C295 at 25564 MHz. This clearly visible beating is from the two bright hotspots, separated by 5 arcsec. (Right) 3C144 at 1040 MHz. The rapid drop to very low visibilities is due to the smooth nebular structure, with no strong gradients.

Table 10
Flux Calibrator Suitability for VLA

Source	Var[a]	MaxFreq[b]	UVRange[c]	Comments
J0133–3629	OK	0.7	0–10	Extremely large and diffuse
3C48	Irreg.	All	0–5000	Can be used up to 40 GHz for VLA
Fornax A	OK	0.2	0–0.05	Generally unsuited for interferometers
3C123	OK	15	0–1000	
J0444–2809	OK	5	0–>50	Probably useful to longer spacings
Pictor A	<4	1.2	0–30	
3C138	Irreg.	All	0–5000	Strongly confused below 500λ at the P band
3C144	Slow	1.2	0–2	Too diffuse for use at high frequencies
3C147	Irreg.	All	0–5000	
3C196	OK	All	0–1000	
3C218	<10	1.5	0–250	
3C274	<4	0.7	0–10	Compact structure could be used at high resn.
3C286	OK	All	0–5000	
3C295	OK	All	0–2000	Too weak at high frequencies and resn.
3C348	OK	3	0–100	
3C353	OK	2	0–20	
3C380	<1?	30	0–5000	Complicated model required
3C405	OK	5	0–250	
3C444	OK	5	0–20	
3C461	Slow	1	0–5	

Notes.
[a] Variability criterion—maximum frequency in GHz for sources with strong nuclei.
[b] Frequency in GHz below which the primary beam resolution criterion is met.
[c] Baseline range (kilowavelengths) to meet confusion, structure, and sensitivity criteria.

considered to be an additional source of noise. The angular size criterion is not critical—if the primary beam shape is known, the attenuation can be calculated since the structure is known. However, this is another model-dependent nuisance, which is best avoided.

These points are illustrated in the following figures. Figure 14 shows the effect of background source confusion of the visibilities for 3C138 at 322 MHz. For this source, the rise in visibility amplitudes at the less than 500 wavelength baseline is due to the Crab Nebula (3C144), located 6.°4 away. The reduction in the confusing visibility is a combination of the resolution of the source, combined with both bandwidth and time averaging of the visibilities. At low frequencies, the confusion from 3C144 makes the short spacings unuseable for calibration. Interferometers shorter than $\sim$1 Kλ (e.g., the VLA in D configuration) should not use this source. The plot shown,

taken from C configuration data, indicates that calibration can be accomplished provided the short spacings are excluded.

The right panel shows the visibility of Cygnus A at 6564 MHz. The source is heavily resolved (and is also large enough that it fails the primary beam resolution criterion), but the longest spacings retain enough visibility that a viable model can be utilized for resolutions at least as good as 5 arcsec.

Figure 15 shows two sources with significant, but very different, resolution effects—3C295 and 3C144. The left panel shows 3C295 at 25564 MHz. Although the source structure comprises two lobes separated by 5 arcsec, the individual lobes are sufficiently small that there is enough visibility on the longest spacings that a stable solution with adequate SNR can be expected for intereferometers with arcsecond resolution. The right panel shows 3C144 at 1040 MHz, with maximum 3 Km baselines. Although the longest spacings are of about 1 Jy flux, which is too small a fraction of the total flux of 900 Jy for a stable solution to be expected.

A summary of the viability of each of the 20 sources for VLA observations is given in Table 10. Note that because many of the criteria are strongly frequency dependent, we have utilized a frequency of 1 GHz. In such cases, the notes column contains additional information.

9. Conclusions

We have defined a comprehensive new flux-density calibration scale for radio astronomy, valid between 50 MHz and 50 GHz. Polynomial coefficients for 20 proposed amplitude scale calibrators, distributed over both hemispheres, and useable both for single dishes and for interferometers of up to a $\sim$5000 Kλ baseline length, are given. The accuracy of this scale is limited by that of the primary calibrator Cygnus A to 3%–5%. The majority of the sources are stable over long periods of time. Some are slowly time variable, and will need regular monitoring to be useful for accurate flux-density calibration.

This scale replaces that proposed by us in 2013 becuase it extends that scale downward from 1 GHz to 50 MHz. The new scale is identical (to the quoted errors) to the old scale above 2 GHz. Correction factors for the older Baars77 scale and the Scaife and Heald scale are given.

The chief weakness of our new scale is at frequencies below 240 MHz. The polynomical expressions are entirely dependent on the two measurements made with the VLA's "legacy" 74 MHz system for 13 of our 20 sources. For the remaining seven sources, there is no VLA measurement, so our expressions for these cannot be used below $\sim$200 MHz. While we have no reason to doubt the accuracy of the old measurements, confidence would be increased when data from the VLA's new low-frequency system, and other low-frequency interferometers, are available.

Probably most useful for confirming the accuracy of our proposed scale would be measurements made by the new generation of low-frequency facilities, notably, the MWA and LOFAR. These would fill the gaps below 250 MHz for our measurements, confirm the ratios that we have determined, and fill in the large gap between 74 and 240 MHz.

A final point worthy of mention is the question of "what calibrates the calibrator"? Our scale at low frequencies is entirely based on observations of Cygnus A with absolutely calibrated antennas and interferometers, nearly all of these were done more than 40 years ago. While we do not doubt the accuracy of these efforts, the availability of modern technologies suggests that more accurate and robust measurements of this fundamental standard should be possible today. Given that the errors of our proposed scale are dominated by the error in the primary calibrators, better accuracy can only be obtained with better fundamental standards.

References

Baars, J. W. M., Genzel, R., Paulinty-Toth, I. K. K., & Witzel, A. 1977, A&A, 61, 99
Baars, J. W. M., & Hartsuijker, A. P. 1983, A&A, 17, 172
Baars, J. W. M., Mezger, P. G., & Wendker, H. 1965, ApJ, 142, 122
Beitenholz, M. B., Kronberg, P. P., Hogg, D. E., & Wilson, A. S. 1991, ApJL, 373, L59
Conway, R. G., Kellermann, K. I., & Long, R. J. 1963, MNRAS, 125, 261
Kassim, N. E., Lazio, T. J. W., Erickson, W. E., et al. 2007, ApJS, 172, 686
Kellermann, K. I. 1964, AJ, 69, 205
Lane, W. M., Clarke, T. E., Taylor, G. B., Perley, R. A., & Kassim, N. E. 2004, AJ, 127, 48
Lister, M. L., Aller, M. F., Aller, H. D., et al. 2013, AJ, 146, 120
Pacholczyk, A. G. 1970, Radio Astrophysics (San Francisco: Freeman)
Partridge, B., Lopez-Caniego, M., Perley, R. A., et al. 2016, ApJ, 821, 61
Perley, R. 2016, EVLA Memo 195
Perley, R. A., & Butler, B. J. 2014, ApJS, 204, 19
Roger, R. S., Bridle, A. H., & Costain, C. H. 1973, AJ, 78, 1030
Scaife, A. M. M., & Heald, G. R. 2012, MNRAS, 423, L30
Wills, B. J. 1973, ApJ, 180, 335